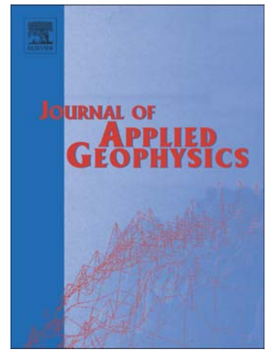

Finite element time domain modeling of controlled-Source electromagnetic data with a hybrid boundary condition

Hongzhu Cai, Xiangyun Hu, Bin Xiong, Esben Auken, Muran Han, Jianhui Li

PII: S0926-9851(17)30087-3
DOI: doi:10.1016/j.jappgeo.2017.08.005
Reference: APPGEO 3321

To appear in: *Journal of Applied Geophysics*

Received date: 19 January 2017
Revised date: 27 July 2017
Accepted date: 16 August 2017

Finite element time domain modeling of controlled-Source electromagnetic data with a hybrid boundary condition

Hongzhu Cai[a], Xiangyun Hu[b], Bin Xiong[c], Esben Auken[d], Muran Han[e], Jianhui Li[b]

[a] *Aarhus University, Department of Geoscience, Aarhus, Denmark (Previously with TechnoImaging, Salt Lake City, Utah, US)*
[b] *China University of Geosciences, Institute of Geophysics and Geomatics, Wuhan, China*
[c] *College of Earth Sciences, Guilin University of Technology, Guilin, Guangxi, China 541004*
[d] *Aarhus University, Department of Geoscience, Aarhus, Denmark*
[e] *University of Utah, Salt Lake City, Utah, USA 84112*

Abstract

We implemented an edge-based finite element time domain (FETD) modeling algorithm for simulating controlled-source electromagnetic (CSEM) data. The modeling domain is discretized using unstructured tetrahedral mesh and we consider a finite difference discretization of time using the backward Euler method which is unconditionally stable. We solve the diffusion equation for the electric field with a total field formulation. The finite element system of equation is solved using the direct method. The solutions of electric field, at different time, can be obtained using the effective time stepping method with trivial computation cost once the matrix is factorized. We try to keep the same time step size for a fixed number of steps using an adaptive time step doubling (ATSD) method. The finite element modeling domain is also truncated using a semi-adaptive method. We proposed a new boundary condition based on approximating the total field on the modeling boundary using the primary field corresponding to a layered background model. We validate our algorithm using several synthetic model studies.

Email addresses: `caihongzhu@hotmail.com` (Hongzhu Cai), `xyhu@cug.edu.cn` (Xiangyun Hu), `hsiungbin@hotmail.com` (Bin Xiong), `esben.auken@geo.au.dk` (Esben Auken), `muran.han@gmail.com` (Muran Han), `ljhiiicumt@126.com` (Jianhui Li)

Keywords: Electromagnetics, marine geophysics, time domain, finite element, backward Euler, direct solver

1. Introduction

The controlled-source electromagnetic (CSEM) methods can be used to provide a resistivity map of the subsurface structure in geophysical exploration (Mulder et al., 2007). This method has been widely adopted in the application of mineral exploration, environmental study, ground water exploration and oil reservoir identification (Fitterman and Stewart, 1986; Ward and Hohmann, 1988; Kamenetsky, 1997; Oh et al., 2015; Persova et al., 2015; Beka et al., 2017). Recently, we also observed a strong interest of using such method in offshore exploration for hydrocarbon reservoir (Constable and Srnka, 2007; Wang et al., 2017). There exist two main categories of CSEM methods: the frequency domain CSEM method and the time domain CSEM method (Ward and Hohmann, 1988; Zhdanov, 2009).

The frequency domain CSEM method has been widely applied in both land and marine environment to map the resistivity structures (Ward and Hohmann, 1988; Connell and Key, 2013). However, the frequency domain electromagnetic (EM) signal is usually dominated by the primary field for typical CSEM survey configurations and this fact leads to a relative small target response (Ward and Hohmann, 1988). Moreover, the air-wave is dominant in land and in shallow marine environments, especially at long source-receiver offsets (Mulder et al., 2007; Key, 2012a; Connell and Key, 2013). The airwave is also coupled with the earth structure which makes the airwave decomposition methods technically difficult (Connell and Key, 2013). The time-domain electromagnetic methods is suggested to overcome these difficulties since the airwave arrives at the early times and the target response from the earth's structures arrives at relatively late-time (Mulder et al., 2007; Connell and Key, 2013; Weiss, 2007; Li, 2010; Jang and Kim, 2015; Sridhar et al., 2017). In addition, the time-domain CSEM method collect data in a similar way to seismic method. The EM data can potentially be integrated with seismic data and the well-developed seismic data processing techniques (e.g., stacking, filtering) can be applied (Strack and Allegar, 2008). It is beneficial to integrate the EM data with seismic data in order to overcome the lower resolution of EM data arising from the diffusive nature of the method (Strack and Allegar, 2008).

Unlike seismic data, the EM signals are diffusive in the conductive earth medium and the direct interpretation of the time-domain EM data is challenging which makes inversion of the data necessary (Mulder et al., 2007). For robust inversion of time-domain EM data, we need an efficient and accurate modeling algorithm (Mulder et al., 2007; Yang et al.,, 2014). The better and more accurate we can simulate the time domain response for realistic earth models, the more useful geological information we can extract from the signals (Sugeng et al., 1993). Comparing to the conventional approach which is to calculate the time-domain response from the transformation of frequency domain solution (Everett and Edwards, 1993; Mulder et al., 2007; Ralph-Uwe et al., 2008), the direct time stepping of Maxwell's equation for electric and magnetic field is preferred, in certain applications, due to its accuracy and computational efficiency (Jin, 2002, 2014; Wang and Hohmann, 1993).

For the direct time stepping approach, the finite difference time domain (FDTD) method has been adopted for decades to solve the electromagnetic diffusion problem in conductive earth medium (Yee, 1966; Sugeng et al., 1993; Wang and Hohmann, 1993; Commer and Newman, 2004; Maaø, 2007). However, the FDTD method is not powerful to simulate complex earth structures (e.g., topography) and the computation domain can be extremely large due to the adoption of regular mesh (Zaslavsky et al., 2011; Um et al., 2012). The unstructured mesh has already been widely used to reduce the computational expense in the application of DC resistivity, plane wave propagation and frequency domain controlled-source electromagnetic modeling both in 2D and 3D (Ansari and Farquharson, 2014; Key and Weiss, 2006; Jahandari et al., 2017; Li and Key, 2007; Rücker et al., 2006; Ren and Tang, 2010; Ren et al., 2013; Tang et al., 2010). The finite element time domain (FETD) method, with unstructured mesh, was proposed to overcome these difficulties in electric engineering (Jin, 2002, 2014). This method was recently introduced to the geophysical community for simulating electromagnetic diffusion problems (Um, 2011; Um et al., 2012; Yin et al., 2016). However, the FETD method requires solving the sparse system of equations at each time stepping for either the explicit or implicit scheme. Fortunately, the developments of computer hardware and the modern direct solver algorithms make it possible to factorize the sparse finite element system of equations efficiently (Jin, 2002, 2014). For the same time stepping size, the FETD stiffness matrix stays unchanged (Jin, 2002, 2014; Um et al., 2012). As a result, the matrix factorization can be reused for the direct solution of the system of equations (Jin, 2002, 2014; Um et al., 2012). In this paper, we consider the FETD formulation with adaptive time step doubling proposed by Um et al. (2012). Within the framework of this approach, the time step size increases with time and the computation cost can be reduced significantly.

For either FDTD or FETD modeling, the Dirichlet boundary is usually adopted (Wang and Hohmann, 1993; Um et al., 2012). For a typical geophysical application, the modeling domain size needs to be tens or hundred km, in each dimension (Um, 2011; Um et al., 2012). The more advanced absorbing boundary conditions (ABC) and the perfectly matched layer (PML) were commonly used to truncate the computation regions in electric engineering (Jin, 2002, 2014; Feng and Liu, 2014). We have observed some trials of using these boundary conditions for geophysical application (Wang and Tripp, 1996; Chen et al.,, 1997). However, these boundary conditions are still not quite applicable to lossy media (Wang and Tripp, 1996; Chen et al.,, 1997) and the implementation of these boundary condition requires significant effort (Jin, 2002, 2014). To address this problem, we approximate the total electric field at different time stage by the primary field corresponding to a layered background conductivity model which can best approximate the full 3D structure (Cai et al., 2017). The primary field in the time domain, for the layered background model, is calculated from the transformation of the frequency domain data obtained using fast Hankel transform (Anderson, 1989; Guptasarma and Singh, 1997; Ward and Hohmann, 1988; Kirkegaard and Auken, 2015). However, the calculated time domain primary field is not accurate for the very earlier stage (Li, 2016). We propose to use the conventional Dirichlet boundary condition with a large modeling domain for the very early modeling stage. Once the FETD solution on the truncated modeling domain boundary produces similar result as the primary field on this boundary, the algorithm will switch to the hybrid boundary condition with the truncated modeling domain. With this method, the computation cost can be reduced significantly.

In the rest part of this paper, we will demonstrate our developed method and algorithm using several typical synthetic model studies.

2. Finite Element Time Domain Discretization of Maxwell's Equation

Consider the quasi-static approximation, we can write the Maxwell's equation in time domain as follows (Ward and Hohmann, 1988; Um et al., 2012):

$$\nabla \times \mathbf{E} = -\mu \frac{\partial \mathbf{H}}{\partial t} \tag{1}$$

$$\nabla \times \mathbf{H} = \mathbf{j_e} + \mathbf{J_s} \tag{2}$$

where $\mathbf{E}$ and $\mathbf{H}$ are electric and magnetic fields. $\mathbf{J_s}$ is source current density and $\mathbf{j_e}$ is the induction current in the conductive earth medium (Ward and Hohmann, 1988; Zhdanov, 2009):

$$\mathbf{j_e} = \widehat{\sigma}\mathbf{E} \tag{3}$$

Here, we consider a general anisotropic earth in our formulation by introducing the electric conductivity tensor $\widehat{\sigma}$ (Cai et al., 2017).

We can eliminate the magnetic field term from the Maxwell's equation and obtain the following diffusion equation (Um et al., 2012):

$$\nabla \times \nabla \times \mathbf{E}(t) + \mu \frac{\partial \mathbf{j_e}(t)}{\partial t} = -\mu \frac{\partial \mathbf{J_s}(t)}{\partial t} \tag{4}$$

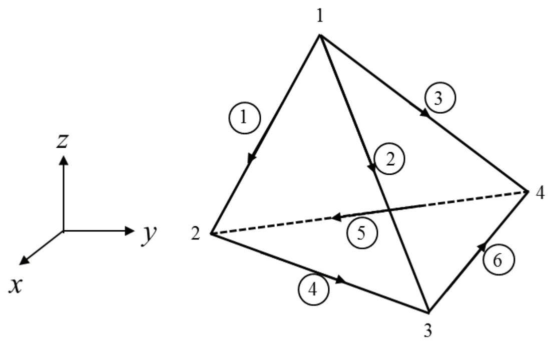

Fig. 1. A tetrahedral element with edge and node definition (Cai et al., 2017).

By substituting (3) into (4), we arrive at the following equation which is ready to be solved using FETD method:

$$\nabla \times \nabla \times \mathbf{E}(t) + \mu\widehat{\sigma}\frac{\partial \mathbf{E}(t)}{\partial t} = -\mu\frac{\partial \mathbf{J_s}(t)}{\partial t} \tag{5}$$

We consider the edge-based finite element (Nédélec, 1980; Jin, 2002, 2014) with a total field formulation and unstructured tetrahedral mesh, as shown in Fig. 1. For the edge-based finite element method, the electric field, at different time stage, is assigned on the element edges and the field inside the element can be calculated from the linear combination of the field on the edges:

$$\mathbf{E}^e(t) = \sum_{i=1}^{6} \mathbf{N}_i^e E_i^e(t). \tag{6}$$

We apply the Galerkin finite element analysis to (5) and obtain a finite element system of equations as follows (Jin, 2002, 2014):

$$K\mathbf{E}(t) + \mu\widehat{\sigma}M\frac{\partial \mathbf{E}(t)}{\partial t} = -\mu M\frac{\partial \mathbf{J_s}(t)}{\partial t} \tag{7}$$

where the stiffness matrix K and M are defined as:

$$K_{ij}^e = \int\limits_{\Omega_e} (\nabla \times \mathbf{N}_i^e) \cdot \left(\nabla \times \mathbf{N}_j^e\right) dv, \tag{8}$$

$$M_{ij}^e = \int\limits_{\Omega_e} \mathbf{N}_i^e \cdot \mathbf{N}_j^e dv, \tag{9}$$

and Ω_e indicates the domain for each element.

We consider a backward Euler scheme, which is unconditionally stable, to calculate the time derivative term in (7) (Ascher and Greif, 2011; Jin, 2002, 2014; Haber, 2014):

$$\frac{\partial \mathbf{E}(t)}{\partial t} \approx \frac{\mathbf{E}(t) - \mathbf{E}(t-\Delta t)}{\Delta t} \tag{10}$$

where Δt is the time-step size.

By substituting this equation into (7), we can obtain:

$$K\mathbf{E}(t) + \frac{\mu\widehat{\sigma}}{\Delta t} M\mathbf{E}(t) = \frac{\mu\widehat{\sigma}}{\Delta t} M\mathbf{E}(t-\Delta t) - \mu M \frac{\partial \mathbf{J_s}(t)}{\partial t} \tag{11}$$

With known initial condition, source waveform and proper boundary condition, the electric field at any time can be obtained by solving (11) in a time stepping manner.

We can further write (11) in a simple form as follows:

$$\mathbf{A}\mathbf{E}(t) = \mathbf{b} \tag{12}$$

where:

$$\mathbf{A} = K + \frac{\mu\widehat{\sigma}}{\Delta t} M, \tag{13}$$

and

$$\mathbf{b} = \frac{\mu\widehat{\sigma}}{\Delta t} M\mathbf{E}(t-\Delta t) - \mu M \frac{\partial \mathbf{J_s}(t)}{\partial t}. \tag{14}$$

3. Hybrid Boundary Condition

Before one can solve the system of equations (12), proper boundary condition needs to be applied to specify the electromagnetic field on the boundary of the modeling domain in order to get a unique solution (Ward and Hohmann, 1988). The homogeneous Dirichlet boundary condition:

$$\mathbf{E}(t)_{\Omega_s} = \mathbf{0}, \tag{15}$$

which assumes the electromagnetic field vanishes on the boundary at all time stage, is the mostly used one due to its simplicity. This type of simple boundary condition generally works effectively for the secondary field formulation considering that the secondary field is relatively small, the modeling domain is reasonably large enough and its boundary is far away from the region filled with anomalous conductivity (Zhdanov, 2009; Silva et al., 2012; Um, 2011; Um et al., 2012). Due to these reasons, the homogeneous Dirichlet boundary has been widely used for the numerical modeling of CSEM data using finite difference, finite volume and finite element methods (Badea et al., 2001; Streich, 2009; Schwarzbach et al., 2011; Um et al., 2012; Silva et al., 2012; Cai et al., 2014).

However, to use the homogeneous Dirichlet boundary condition for the total field formulation, one has to set a relatively large modeling domain (Ward and Hohmann, 1988; Jahandari and Farquharson, 2014; Haber et al., 2007; Haber, 2014). One need to note that the size of a modeling domain also depends on the moment of the source (Cai et al., 2017). The same grid may work for a survey with lower source moment but it may not work anymore if one increase the source moment. In addition, the electric field on the modeling domain boundary also changes with time for FETD modeling (Jin, 2002, 2014). As a result, the application of the conventional Dirichlet boundary condition can be problematic.

We propose to use a new boundary condition which approximate the total field on the domain boundary by the primary field. We define a layered background conductivity model which can best approximate the actual 3D conductivity. As a result, the background model contains the averaged conductivity information of the actual 3D model. We define the primary field as the electromagnetic response excited by the source in the background conductivity model. In our algorithm, we can either specify this background conductivity model in input file or let the algorithm calculate it automatically. Based on our numerical tests, we find that this type of boundary condition works much more efficiently than the homogeneous Dirichlet boundary condition. The size of the modeling domain can be reduced dramatically. In addition, the size of the modeling domain becomes irrelevant with the source moment.

Fig. 2 shows a 2D illustration of this hybrid boundary condition (our method is actually for a general 3D case). For the conventional homogeneous Dirichlet boundary condition, we have to use a large domain A with boundary of Ω_A.

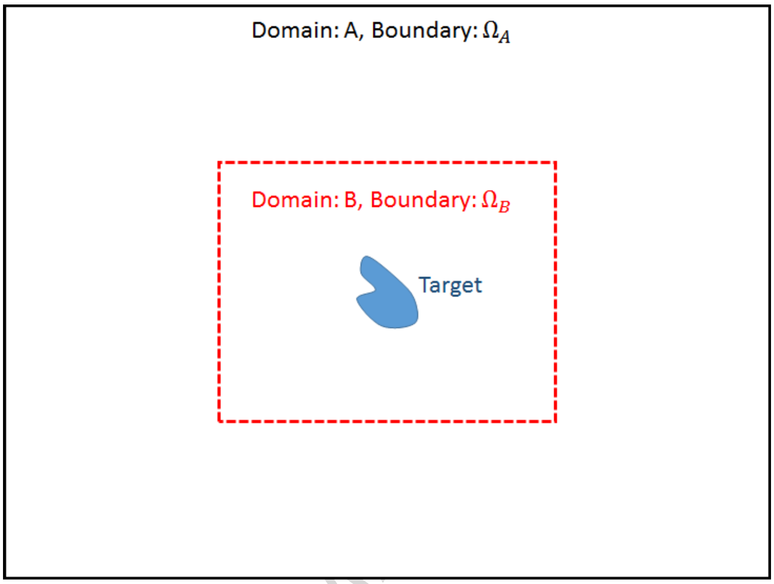

Fig. 2. 2D illustration of modeling domain truncation and the hybrid boundary condition.

Instead, we can use a small modeling domain B with boundary of Ω_B. In this case, we approximate the time-domain electric field on Ω_B by the primary field corresponding to a layered background model.

This approach has been demonstrated to be effective for frequency domain EM modeling (Cai et al., 2017) where the optimized truncation domain Ω_B can be decided in a semi-adaptive manner (Cai et al., 2017). For a specific frequency, we can start from a small modeling domain and gradually increase the domain size. We can do forward modeling for these different domains (from the smallest one) and terminate the process until the solution difference reaches the tolerance. For one frequency, the solution for a small domain can be obtained very quickly and the computation cost for this process is low (Cai et al., 2017). However, this adaptive approach cannot be directly applied to time domain, since the computational cost in each small domain is much more expensive than for frequency domain modeling. In this paper, the size of the truncated domain is obtained based on experience.

As we mentioned before, the calculated time domain primary field on the boundary of the truncated domain is not accurate for the earlier stage due to the limitation of digital filter used for the frequency-time domain transformation (Key, 2012b; Li, 2016). As a result, one need to be cautious to apply such hybrid boundary condition. To overcome this problem, we decide to use a dual domain modeling method as shown in Fig. 2. For the earlier stage, we use a large domain A with homogeneous Dirichlet boundary condition. Once the difference between the primary field and the FETD solution, simulated with homogeneous Dirichlet boundary condition and larger domain, on boundary Ω_B is within the preselected tolerance ϵ, we will switch to the hybrid boundary condition with a smaller modeling domain of B.

4. Initial Condition and Solution of FETD System

Before applying the time stepping process, we need to specify the initial condition based on the source waveform. In this paper, we adopt the impulse source which is approximated by a Gaussian function as shown in Fig. 3. For this type of source waveform, a zero initial condition can be used (Um et al., 2012). Actually, our algorithm can take the arbitrary waveform as input. The initial time stepping size depends on the discretization of the source waveform. With the discussed initial and boundary condition, the system of equation (12) is ready to be solved. It has been shown that we have to solve the system at each step for FETD formulation (Jin, 2002, 2014). It will be unrealistic to solve such system using iterative solver considering the number of time stepping could be large (Jin, 2002, 2014; Um et al., 2012). It has been shown that the FETD stiffness matrix stays the same if we use the same time stepping size of Δt. In this scenario, it may be reasonable to use a direct solver since the matrix factorization can be reused if we keep the same time stepping size (Jin, 2002, 2014; Oldenburg et al., 2012). In this paper, we use the direct solver package SuiteSparse v4.5.3 with a MATLAB interface (Davis, 2006) to solve the system of equations.

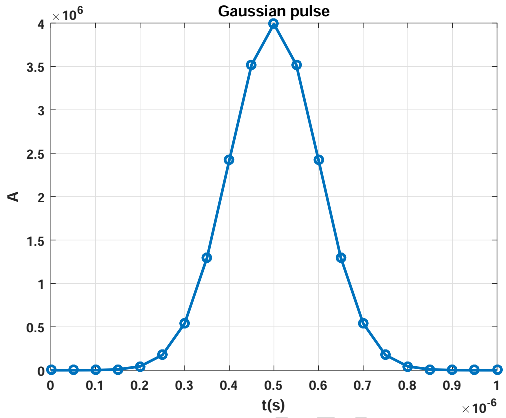

Fig. 3. Approximation of the impulse source waveform with Gaussian pulse.

However, the number of time steps will be significantly large if we keep Δt unchanged since a small time stepping size is required in the earlier stage (Um et al., 2012). To solve this problem, we consider an adaptive time stepping doubling methods (Um et al., 2012) to gradually increase the time stepping size. Within the framework of this approach, we keep the same time stepping size Δt for a fixed number of steps (e.g., 100 step) and then try to increase the time step size to $2\Delta t$. If the difference between the FETD solution for these two different time step size is smaller than the tolerance, the time stepping doubling will be accepted and vice versa (Um, 2011; Um et al., 2012). If the time stepping doubling is rejected, the matrix factorization for the FETD matrix with step size of $2\Delta t$ can still be saved for the next time stepping doubling trial. It has been demonstrated that the time stepping process can be speeded up dramatically by adopting the ATSD (adaptive time step doubling) method (Um et al., 2012).

5. Model Studies

In this section, we will validate the developed algorithm by several model studies. For simplicity, we consider the electric dipole source. The more complicated source geometry (e.g., long wire and loop) can be constructed from integration of electric dipoles (Ward and Hohmann, 1988; Cai et al., 2017) and will be studied in the future. We first consider a halfspace model with the electric dipole source located at the air-earth interface such that the solution of the EM signal at the receiver has a closed form. Following this, we consider a 3D anomaly embedded in the half space background. For the frequency-time domain transformation, we use the method in Key (2012b) with 101 frequencies uniformly spaced from 10^{-5} Hz to 10^{5} Hz in logarithmic space. Finally, we demonstrate our algorithm by the more realistic SEG marine salt model with complex bathymetry. We run the algorithm on a PC desktop with 4 cores (i7-6700K) and 64 GB memory.

5.1. Halfspace model

We first consider the electromagnetic diffusion in a halfspace earth, with the resistivity of $500\Omega \cdot m$, excited by an electric dipole located at $(-1000, 0, 0)$m. We use the same source waveform as shown in Fig. 3. The source waveform discretization results in an initial time step size of 5×10^{-8}s. We simulate the electromagnetic response from $t = 0$ to $t = 1s$.

As mentioned, we use a dual modeling domain during this simulation. In the earlier stage, we use a large modeling domain with a size of $50km \times 50km \times 50km$. Such relative large domain contains 312,551 elements and 371,328 edges. In the late stage, we use a smaller modeling domain with the size of $4km \times 4km \times 4km$. The smaller domain (truncated domain) contains 68,705 elements and 81,358 edges. The homogeneous Dirichlet boundary condition and the proposed hybrid boundary condition are applied to the larger and smaller modeling domain, respectively. The total computation time is around 400 s for the dual-modeling domain approach with the proposed hybrid boundary condition. However, it takes around 25 minutes to finish the calculation if we choose the homogeneous Dirichlet boundary condition with the large modeling domain. The total number of time steps is 1773 with the ATSD method. Fig. 4 shows that the time step size increases with time. The total number of steps would be 2×10^{7} if we use a uniform time step size of 5×10^{-8}.

Fig. 5 shows the inline electric field on the earth's surface calculated from an

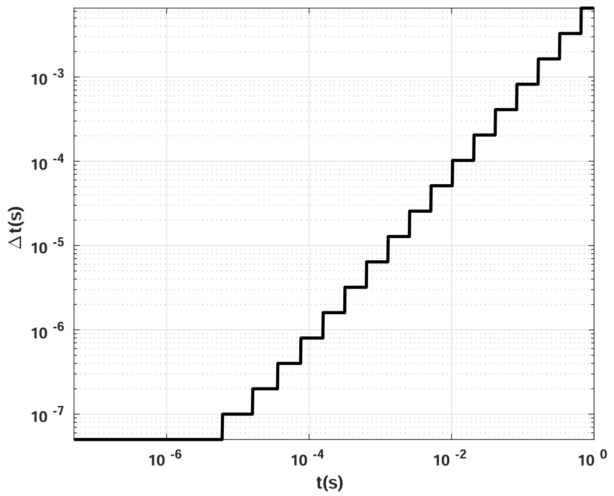

Fig. 4. Adaptive time step size for the halfspace model.

analytical solution (see equation (A.8)) and FETD method with the proposed hybrid boundary condition at two different offsets. We can see that the FETD solution compares well to the analytical solution in both earlier and late-time. Fig. 6 shows the inline electric field on the earth's surface calculated from the analytical solution and the FETD method with the conventional zero Dirichlet boundary condition at two different offsets. From this figure, we can clearly see that the difference between the FETD solution and the analytical for late-time, although we used a relative large modeling domain for the zero Dirichlet boundary condition.

Fig. 7 shows the sparsity pattern of the FETD stiffness matrix for the modeling with conventional zero Dirichlet boundary condition and the hybrid boundary condition. We can see that the number of non-zeros for the conventional zero Dirichlet boundary condition case is almost 5 times as the case with the proposed hybrid condition. It is clear that the computational expense and memory cost can be reduced significantly by adopting this hybrid boundary condition. In the meantime, the numerical accuracy is improved dramatically. Furthermore, we want to emphasize that for the conventional zero Dirichlet boundary con-

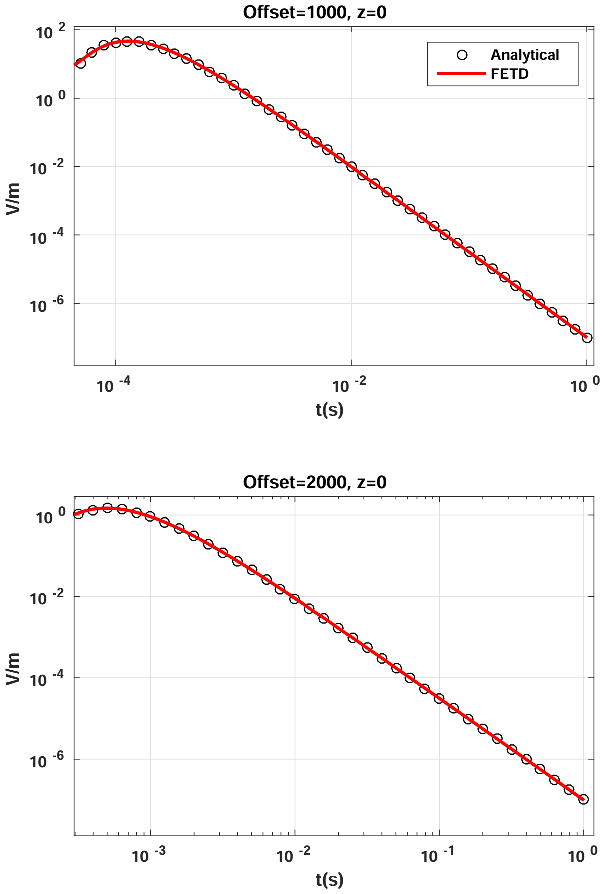

Fig. 5. A comparison between the inline electric field component, E_x, calculated from analytical solution and FETD method with the hybrid boundary condition for the halfspace model at the offsets of 1000m and 2000 m.

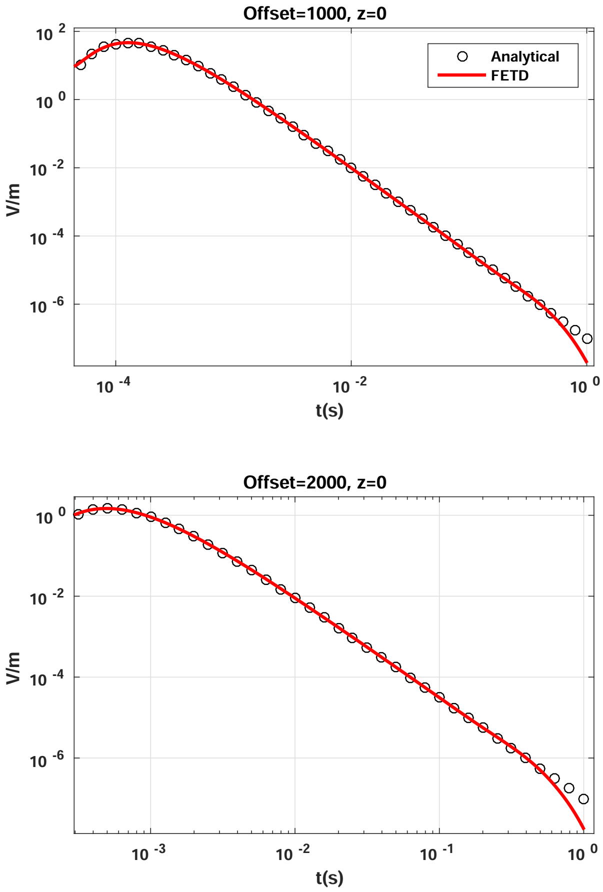

Fig. 6. A comparison between the inline electric field component, E_x, calculated from analytical solution and FETD method with the conventional zero Dirichlet boundary condition for the halfspace model at the offsets of 1000m and 2000 m.

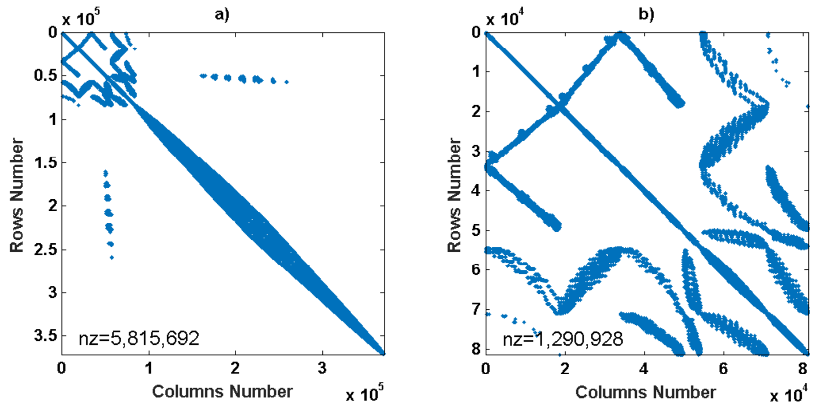

Fig. 7. Panel a) shows the sparsity pattern of stiffness matrix for the FETD method with the conventional zero Dirichlet boundary condition; panel b) shows the sparsity pattern of stiffness matrix for the FETD method with the proposed hybrid boundary condition. The parameter nz in each panel represents the number of no-zeros in the stiffness matrix.

dition, the modeling domain also depends on the source moment. A modeling domain works for small source moment may not work anymore if we increase the source moment (Cai et al., 2017). However, within the framework of the proposed hybrid boundary condition, the size of the domain truncation actually does not depends on the source moment.

5.2. 3D model with flat surface

We now consider a 3D model with two anomalous bodies embedded in the halfspace earth with a resistivity of $500\Omega \cdot m$. Fig. 8 is an illustration of this

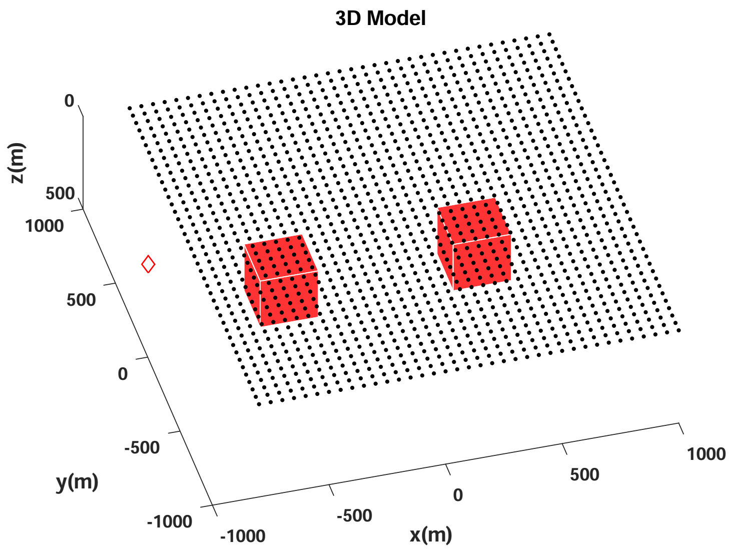

Fig. 8. Illustration of the 3D model. The red cubes are the anomalous bodies. The black dots represent the receivers while the red diamond shape in the left indicates the location of the electric dipole source.

model. The size of these two anomalous bodies are $250m \times 250m \times 250m$. The resistivity of the left body is $1\Omega{\cdot}m$ while the resistivity of the right body is $0.2\Omega{\cdot}m$. The center location of these two bodies are located at $(-400, 100, 300)$m and $(400, 0, 200)$m, respectively. The x oriented electric dipole source is located at $(-1000, 0, 0)$m.

We use the hybrid boundary condition for this model and the finite element modeling domain is the same as the previous halfspace model. However, we refined the mesh inside the anomalous bodies and the observation surface. The tetrahedral mesh for the large domain contains $306,908$ elements and $361,763$ edges. The tetrahedral mesh for the truncated domain contains $185,801$ elements and $220,408$ edges. The total computation time for this model is around 10 minutes.

For comparison, we also compute the time domain response using the cosine transform and the frequency domain response is calculated using a frequency

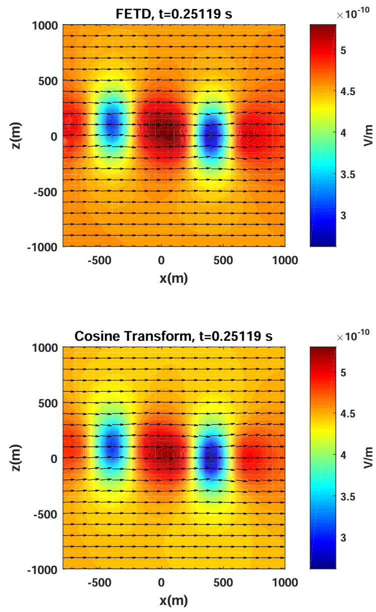

Fig. 9. FETD solution and the frequency domain transformed solution for the 3D model with a flat surface. The arrows represent the direction of the electric field on the surface.

domain FEM code (Cai et al., 2017). Fig. 9 shows the electric field, on the earth's surface at $t{\approx}0.25s$, calculated with the FETD method and the cosine transform, respectively. We can see that the FETD solution compares well with the frequency-domain transformed result. Fig. 10 shows the electric field, at $t{\approx}0.25s$, on the vertical plane of $y = 0$.

Fig. 11 shows the time domain response of the electric field at the location of $(-400, 0, 0)$ m, which is directly above the left anomalous body. In this figure, we also present the comparison between the FETD solution and the frequency domain transformed result, at one station. We can see that the FETD solution matches well with the frequency domain transformed solution at different time stages. In addition, we compared the results with the halfspace response (dashed black line). We can clearly see the distortion from the 3D bodies. At this

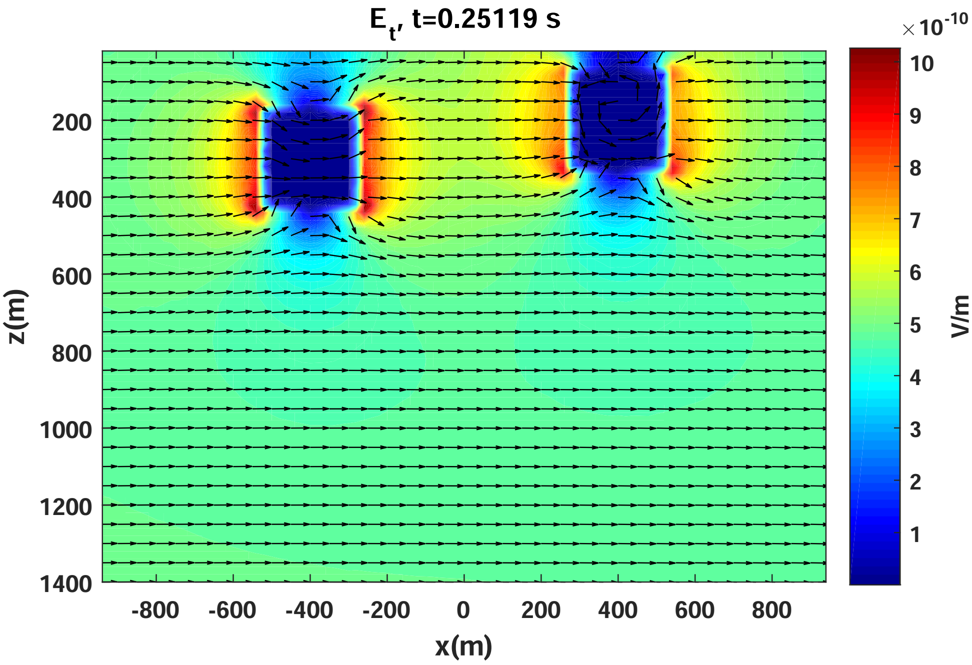

Fig. 10. FETD solution, for the 3D model with a flat surface, on the plane of $y = 0$. The arrows represent the direction of the electric field on this plane.

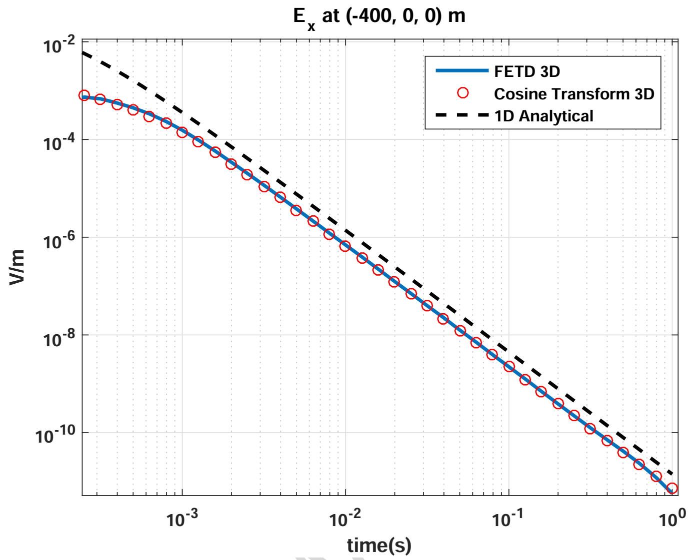

Fig. 11. Time domain response of electric field at $x = -400$ m, $y = 0$ and $z = 0$.

sounding station, which is above the left anomalous body, the size of the body is relative large comparing to the source-receiver offset, the EM response is affected significantly by the target even in the late-time.

Fig. 12 shows the time domain response of the electric field at the location of $(1000, 0, 0)$ m. It shows the EM response for the case with and without 3D anomaly. In the case of without 3D anomaly, the solution is calculated both with the analytical method and FETD method (we use exact the same mesh as the case with 3D anomaly). We see that the halfspace response calculated from analytical solution (black dots) is almost identical with the solution from the FETD method (solid blue line). By doing this comparison, we can further validate that the selected mesh grid and modeling domain is proper and will not cause artificial anomalies. The dashed red line in Fig. 12 represents the EM response for the model with 3D anomalies. At this sounding station, the source-receiver offset is relative much larger comparing to the dimension of the 3D anomalies and the receiver is at some distance from the anomalous bodies, the 3D model response converges, as expected, to the halfspace response at late-time channels.

6. Realistic marine salt dome model

Finally, we consider a marine CSEM model with complex bathymetry and a salt structure (Aminzadeh et al., 1996) that we used in our previous publication (Cai et al., 2017). Fig. 13 shows an illustration of this model.

This model contains multiple geological layers characterized by resistivity anisotropy. The resistivity of the seawater is $3.3\Omega \cdot m$. The horizontal and vertical resistivity of sediments are $1\Omega \cdot m$ and $1.25\Omega \cdot m$, respectively. The horizontal and vertical resistivity of the basement rock, underlie the sediments, are $10\Omega \cdot m$ and $20\Omega \cdot m$. The salt structure is resistive with a horizontal and vertical resistivity of $100\Omega \cdot m$ and $500\Omega \cdot m$, respectively. We consider several x oriented electric dipole sources towed above the seafloor. Because we adopt the direct solver, the matrix only needs to be factorized once for all sources. As a result, the number of sources will not increase the calculation time significantly. We will only show the results for the electric dipole source located at $(-4000, 0, 800)$ m. The source waveform is the same as the previous models.

The optimized truncated modeling domain size is $16km \times 14km \times 14km$ and the unstructured discretization of this truncated domain results in 548,419 elements and 465,904 edges. The size of the large domain with homogeneous Dirichlet boundary condition is $60km \times 60km \times 60km$ and the corresponding unstructured mesh contains 691,169 elements and 813,504 edges. The total computation for running this model is around 36 minutes. However, it takes around 2 hours to solve it with a large domain and the Dirichlet boundary condition. In addition, the large domain with 813,504 edges almost reaches the limits of the SuiteSparse solver.

Fig. 14 shows a comparison between the FETD solution and the transformation from the frequency domain result (Cai et al., 2017) at one receiver location. We can see the FETD result compares well with the frequency domain trans-

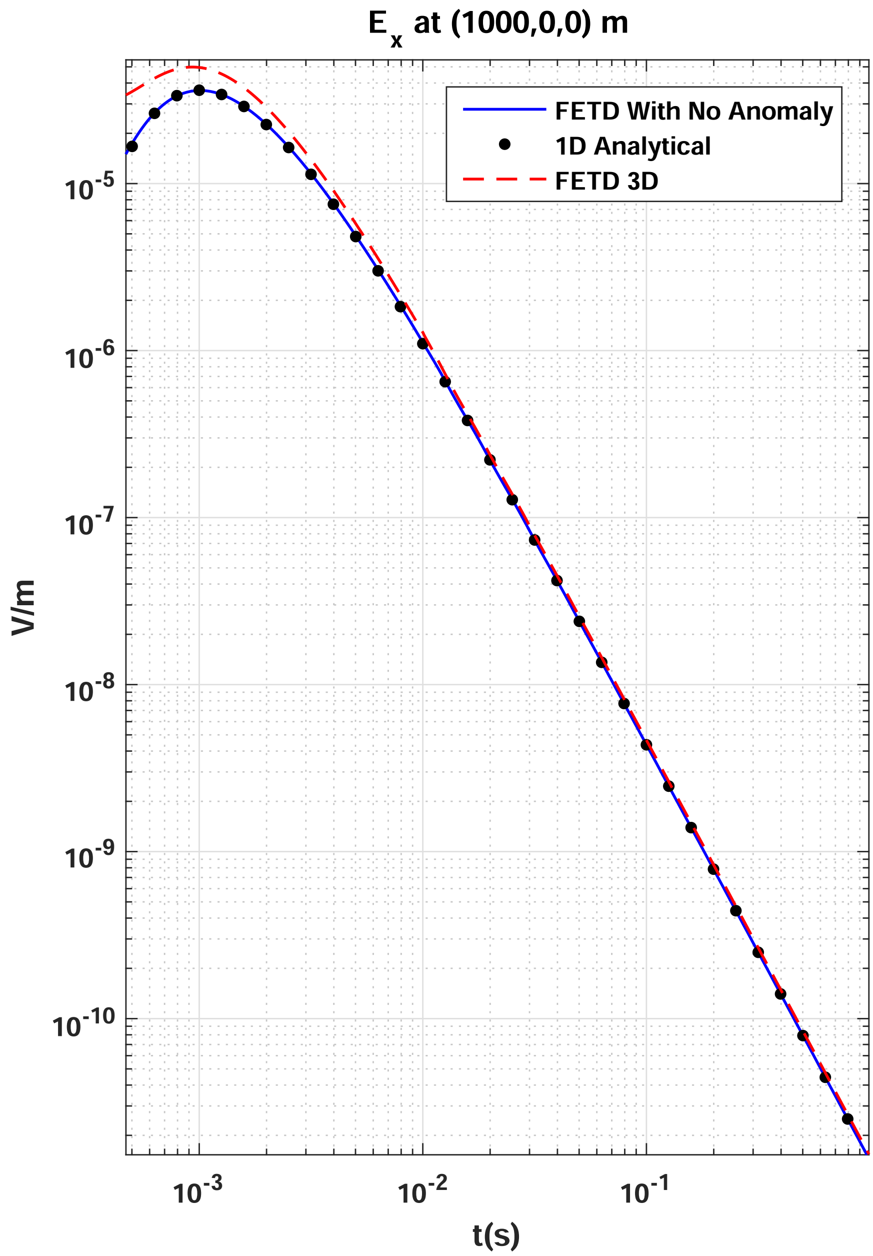

Fig. 12. Time domain response of electric field at $x = 1000$ m, $y = 0$ and $z = 0$.

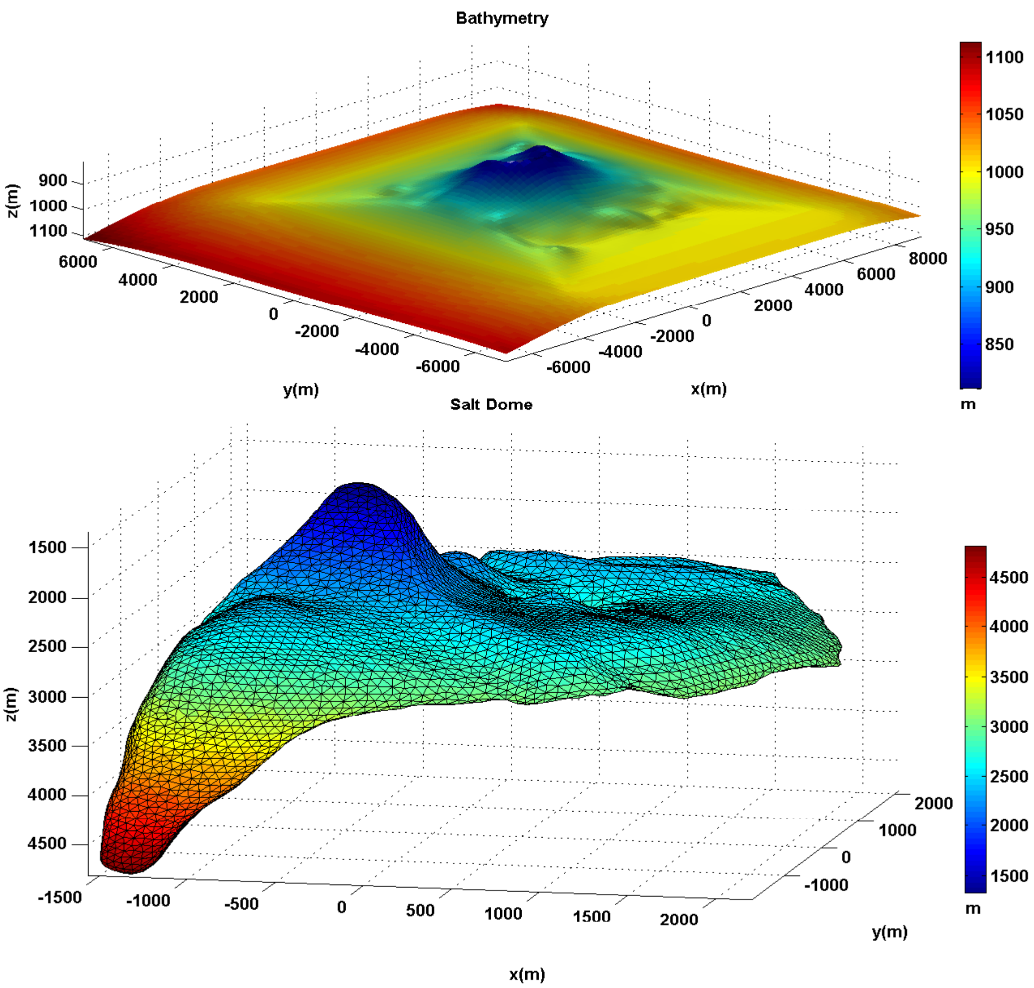

Fig. 13. SEG salt dome model with complex bathymetry. The lower panel shows the surface discretization of the salt (Cai et al., 2017).

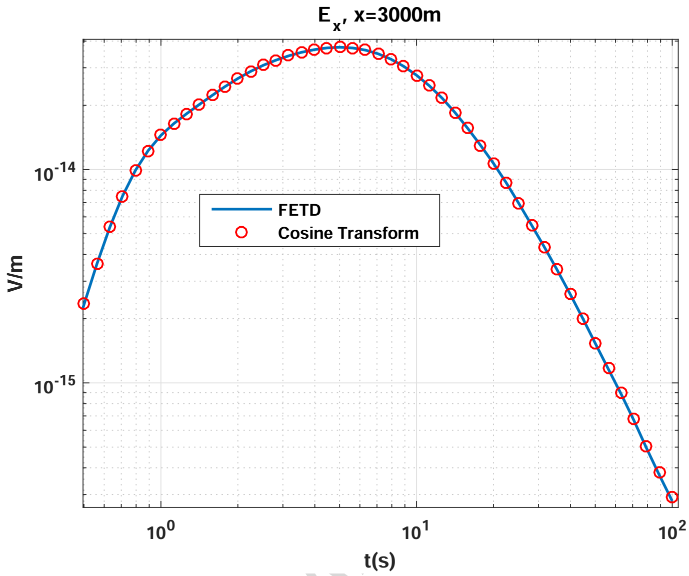

Fig. 14. A comparison between FETD solution and the frequency domain transformed solution for the salt dome model, at $x = 3000$ and $y = 0$.

formed result for this complex model. The FETD solution also compares well to the frequency domain transformed solution for all other receivers.

We also computed the total field with bathymetry but without the salt dome response. Fig. 15 shows a comparison between the total field, layered background response and the total field without salt dome, at $x = 3000$ and $y = 0$. From this figure, we can clearly see the distortion caused by bathymetry and the salt dome from $t = 1s$ to $t = 10s$.

We can normalize the total field by some background field to get the normalized anomaly which can reflect the distortion from the target. We normalize the total field by the layered background response and also by the bathymetry background. We define the bathymetry background as the total field for the model with bathymetry but without the salt dome. Fig. 16 shows a comparison between these two different normalized anomalies. We can see that the normalized anomaly can be overestimated without carefully considering the bathymetry effects.

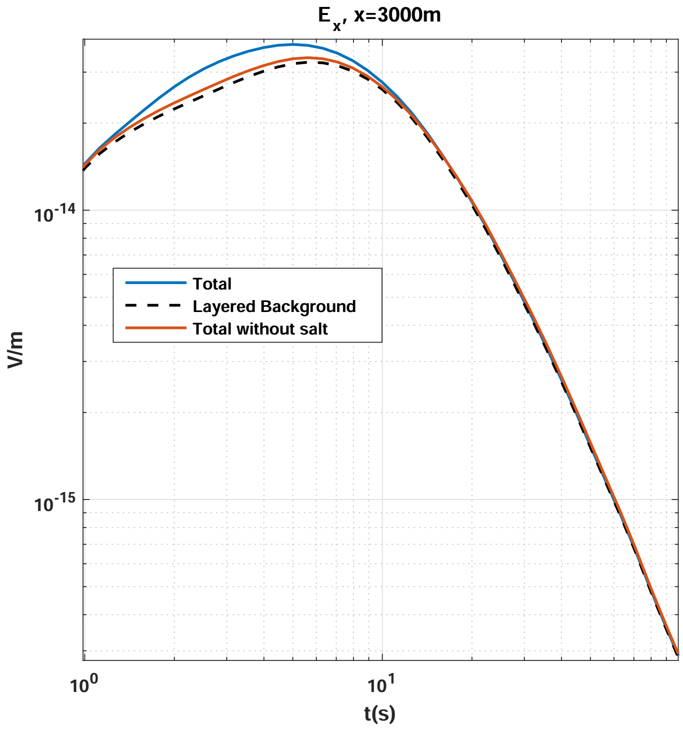

Fig. 15. The time domain response of the electric field, at $x = 3000$ and $y = 0$, for different scenarios.

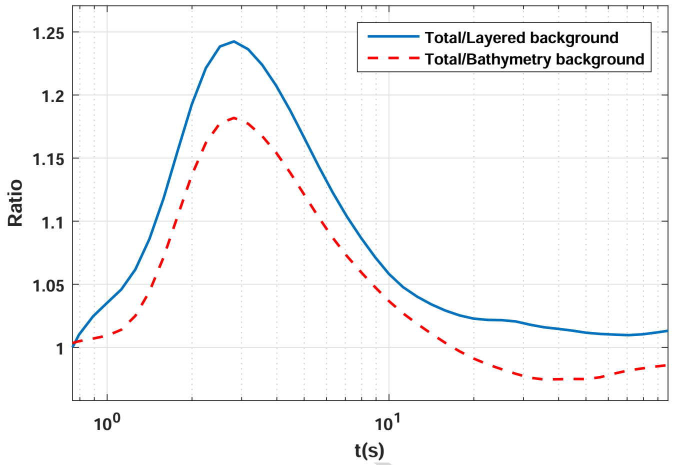

Fig. 16. Normalized anomaly of the time domain electric field, at $x = 3000$ and $y = 0$, by different background field.

Finally, we calculate the time domain response for this model with isotropic resistivity by setting the resistivity as the horizontal resistivity in all area. Fig. 17 shows a comparison between the time domain response for this model with isotropic and anisotropic resistivity. We can see that the time domain response is distorted remarkably by the anisotropic effects.

7. Conclusions

We have developed a 3D edge-based finite element time domain modeling algorithm for solving electromagnetic diffusion problem in conductive earth medium. The diffusive equation is discretized using a backward Euler scheme which is unconditionally stable. The sparse system of equation is solved using the direct method based on LU decomposition and as a result the matrix factorization can be reused for the same time stepping size. We also consider an adaptive time step doubling scheme to gradually increase the time step size. The modeling domain is discretized using unstructured tetrahedral mesh to reduce the size of the problem and simulate complex geometry.

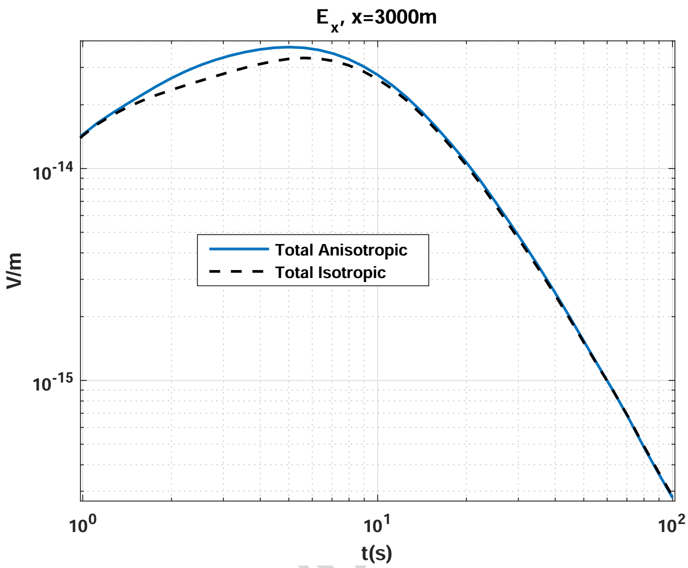

Fig. 17. A comparison between the time domain response of the electric field, at $x = 3000$ and $y = 0$, for the isotropic and anisotropic model.

We consider a total field formulation for the electric field. Comparing to the conventional homogeneous Dirichlet boundary condition, we proposed a hybrid boundary condition. The electric field on the truncated domain boundary is assumed to be the same as the primary field corresponding to a layered earth model which can best approximate the actual 3D model. As a result, this boundary condition for the total field formulation is equivalent to the Dirichlet boundary condition with a secondary field formulation. We have demonstrated that the application of this type of boundary condition can reduce the computation cost significantly. Within the framework of this approach, the primary field on the truncated domain boundary is calculated in frequency domain and transformed to time domain using digital filter. Such transformation can result in incorrect result for the earlier stage. We have proposed a dual modeling domain approach to address this problem. In the earlier stage, we still use a larger modeling domain with the Dirichlet boundary condition. With time increase, the algorithm will automatically switch to the truncated domain and the proposed boundary condition.

We have validated the proposed method and algorithm using several synthetically models. The numerical studies show that our algorithm can produce accurate result for typical time domain CSEM modeling and the code is capable of simulating realistic models with complex topography. Our future work includes parallelizing the algorithm for large scale modeling.

8. Acknowledgement

The authors are thankful to Professor Ren and another anonymous reviewer for their valuable suggestions.

References

Anderson, W.L., 1989. A hybrid fast hankel transform algorithm for electromagnetic modeling, *Geophysics.* **54**, 263–266.

Aminzadeh, F., Burkhard, N., Long, J., Kunz, T. and Duclos, P., 1996. Three dimensional SEG/EAEG models-an update, *The Leading Edge.* **15**, 131-134.

Ascher U. M. and Greif C., 2011. *A first course in numerical methods*, SIAM.

Ansari, S. and Farquharson, C.G., 2014. 3D finite-element forward modeling of electromagnetic data using vector and scalar potentials and unstructured grids, *Geophysics.* **79**, E149-E165.

Badea, E.A., Everett, M.E., Newman, G.A. and Biro, O., 2001. Finite-element analysis of controlled-source electromagnetic induction using Coulomb-gauged potentials, *Geophysics.* **66**, 786-799.

Beka, T.I., Senger, K., Autio, U.A., Smirnov, M. and Birkelund, Y., 2017. Integrated electromagnetic data investigation of a Mesozoic CO2 storage target reservoir-cap-rock succession, Svalbard, *Journal of Applied Geophysics.* **136**, 417-430.

Chen, Y.H., Chew, W.C. and Oristaglio, M.L., 1997. Application of perfectly matched layers to the transient modeling of subsurface EM problems, *Geophysics*. **62**, 1730-1736.

Commer, M. and Newman, G., 2004. A parallel finite-difference approach for 3D transient electromagnetic modeling with galvanic sources, *Geophysics*. **69**, 1192-1202.

Constable, S. and Srnka, L.J., 2007. An introduction to marine controlled-source electromagnetic methods for hydrocarbon exploration, *Geophysics*. **72**, WA3-WA12.

Connell, D. and Key, K., 2013. A numerical comparison of time and frequencydomain marine electromagnetic methods for hydrocarbon exploration in shallow water, *Geophys. Prospect.*. **61**, 187-199.

Cai, H., Xiong, B., Han, M. and Zhdanov, M., 2014. 3D controlled-source electromagnetic modeling in anisotropic medium using edge-based finite element method, *Computers & Geosciences*. **73**, 164–176.

Cai, H., Cuma, M. and Zhdanov, M.S., 2015, Three-Dimensional Parallel Edge-Based Finite Element Modeling of Electromagnetic Data with Field Redatuming, *85th Annual International Meeting, SEG, Expanded Abstract*. 1012–1017.

Cai, H., Hu, X., Li, J., Endo, M. and Xiong, B., 2017. Parallelized 3D CSEM modeling using edge-based finite element with total field formulation and unstructured mesh, *Computers & Geosciences*. **99**, 125-134.

Davis, T., 2006. *Direct methods for sparse linear systems*, SIAM.

Everett, M.E. and Edwards, R.N., 1993. Transient marine electromagnetics: The 2.5-D forward problem, *Geophys. J. Int.*. **113**, 545-561.

Fitterman, D.V. and Stewart, M.T., 1986. Transient electromagnetic sounding for groundwater, *Geophysics*. **54**, 995-1005.

Feng, N. and Liu, Q.H., 2014. Efficient implementation of multi-pole UPML using trapezoidal approximation for general media, *Journal of Applied Geophysics*. **111**, 59-65.

Guptasarma, D., Singh, B., 1997. New digital linear filters for Hankel J0and J1 transforms, *Geophys. Prospect.*. **54**, 263–266.

Haber, E., Oldenburg, D.W. and Shekhtman, R., 2007. Inversion of time domain three-dimensional electromagnetic data, *Geophys. J. Int.*. **171**, 550-564.

Haber, E., 2014. *Computational methods in geophysical electromagnetics (Vol. 1)*, SIAM.

Jin, J., 2002. *Finite element method in electromagnetics, Second Edition*, Wiley-IEEE Press.

Jin, J., 2014. *Finite element method in electromagnetics, Third Edition*, Wiley-IEEE Press.

Jang, H. and Kim, H.J., 2015. Mapping deep-sea hydrothermal deposits with an in-loop transient electromagnetic method: Insights from 1D forward and inverse modeling, *Journal of Applied Geophysics*. **123**, 170-176.

Jahandari, H. and Farquharson, C.G., 2014. A finite-volume solution to the geophysical electromagnetic forward problem using unstructured grids, *Geophysics*. **79**, E287-E302.

Jahandari, H., Ansari, S. and Farquharson, C.G., 2017. Comparison between staggered grid finitevolume and edgebased finiteelement modelling of geophysical electromagnetic data on unstructured grids, *Journal of Applied Geophysics*. **138**, 185-197.

Kamenetsky, F.M., 1997. *Transient geo-electromagnetics*, GEOS.

Key, K. and Weiss, C., 2006. Adaptive finite-element modeling using unstructured grids: The 2D magnetotelluric example, *Geophysics*. **71**, G291-G299.

Key, K., 2012. Marine electromagnetic studies of seafloor resources and tectonics, *Surveys in geophysics.* **33**, 135-167.

Key, K., 2012. Is the fast Hankel transform faster than quadrature?, *Geophysics.* **77**, F21-F30.

Kirkegaard, C. and Auken, E., 2015. A parallel, scalable and memory efficient inversion code for very largescale airborne electromagnetics surveys, *Geophys. Prospect..* **63**, 495-507.

Li, Y. and Key, K., 2007. 2D marine controlled-source electromagnetic modeling: Part 1 – An adaptive finite-element algorithm, *Geophysics.* **72**, WA51-WA62.

Li, Y. and Constable, S., 2010. Transient electromagnetic in shallow water: insights from 1D modeling, *Chinese Journal of Geophysics-Chinese Edition.* **53**, 737-742.

Li, J., Farquharson, C.G. and Hu, X., 2016. Three effective inverse Laplace transform algorithms for computing time-domain electromagnetic responses, *Geophysics.* **81**, E113-E128.

Meerschaert, M.M. and Tadjeran, C., 2004. Finite difference approximations for fractional advectiondispersion flow equations, *Journal of Computational and Applied Mathematics.* **172**, 65-77.

Maaø, F.A., 2007. Fast finite-difference time-domain modeling for marine-subsurface electromagnetic problems, *Geophysics.* **72**, A19-A23.

Mulder, W.A., Wirianto, M. and Slob, E.C., 2007. Time-domain modeling of electromagnetic diffusion with a frequency-domain code, *Geophysics.* **73**, F1-F8.

Nédélec, J.C., 1980. Mixed finite elements in R^3, *Numer. Math..* **35**, 315–341.

Oldenburg, D.W., Haber, E. and Shekhtman, R., 2012. Three dimensional inversion of multisource time domain electromagnetic data, *Geophysics.* **78**, E47-E57.

Oh, S., Noh, K., Seol, S.J., Byun, J. and Yi, M.J., 2016. Interpretation of controlled-source electromagnetic data from iron ores under rough topography, *Journal of Applied Geophysics*. **124**, 106-116.

Persova, M.G., Soloveichik, Y.G., Domnikov, P.A., Vagin, D.V. and Koshkina, Y.I., 2015. Electromagnetic field analysis in the marine CSEM detection of homogeneous and inhomogeneous hydrocarbon 3D reservoirs, *Journal of Applied Geophysics*. **119**, 147-155.

Rücker, C., Günther, T. and Spitzer, K., 2006. Three-dimensional modelling and inversion of DC resistivity data incorporating topographyI. Modelling, *Geophys. J. Int.*. **166**, 495-505.

Ralph-Uwe, B., Ernst, O.G. and Spitzer, K., 2008. Fast 3-D simulation of transient electromagnetic fields by model reduction in the frequency domain using Krylov subspace projection, *Geophys. J. Int.*. **173**, 766-780.

Ren, Z. and Tang, J., 2010. 3D direct current resistivity modeling with unstructured mesh by adaptive finite-element method, *Geophysics*. **75**, H7-H17.

Ren, Z., Kalscheuer, T., Greenhalgh, S. and Maurer, H., 2013. A goal-oriented adaptive finite-element approach for plane wave 3-D electromagnetic modelling, *Geophys. J. Int.*. **194**, 700-718.

Sugeng, F., Raiche, A. and Rijo, L., 1993. Comparing the Time-Domain EM Response of 2-D and Elongated 3-D Conductors Excited by a Rectangular Loop Source, *Journal of geomagnetism and geoelectricity*. **45**, 873-885.

Strack, K.M. and Allegar, N., 2008. Marine time domain CSEM: an emerging technology, *78rd Annual International Meeting, SEG, Expanded Abstract*. 653–656.

Streich, R., 2009. 3D finite-difference frequency-domain modeling of controlled-source electromagnetic data: Direct solution and optimization for high accuracy, *Geophysics*. **75**, F95F105.

Schwarzbach, C., Börner, R.U., Spitzer, K., 2011. Three-dimensional adaptive higher order finite element simulation for geo-electromagnetics–a marine CSEM example, *Geophys. J. Int.*. **187**, 63–74.

Silva, N.V., Morgan, J.V., MacGregor, L., Warner, M., 2012. A finite element multifrontal method for 3D CSEM modeling in the frequency domain, *Geophysics.* **77**, E101–E115.

Sridhar, M., Markandeyulu, A. and Chaturvedi, A.K., 2017. Mapping subtrappean sediments and delineating structure with the aid of heliborne time domain electromagnetics: Case study from Kaladgi Basin, Karnataka, *Journal of Applied Geophysics.* **136**, 9-18.

Tang, J.T., Wang, F.Y. and Ren, Z.Y., 2010. 2.5-D DC resistivity modeling by adaptive finite-element method with unstructured triangulation, *Chinese J. Geophys.* **53**, 708-716.

Tu, X., 2015. *Time domain approach for multi-channel transient electromagnetic modeling*, Master Thesis, University of Chinese Academy of Sciences.

Um, E.S., 2011. *Three-dimensional finite-element time-domain modeling of the marine controlled-source electromagnetic method*, Ph.D dissertation, Stanford University.

Um, E.S., Harris, J.M. and Alumbaugh, D.L., 2012. An iterative finite element time-domain method for simulating three-dimensional electromagnetic diffusion in earth, *Geophys. J. Int.*. **190**, 871-886.

Ward, S.H., Hohmann, G.W., 1988. *Electromagnetic Theory for Geophysical Applications:*, SEG.

Wang, T. and Hohmann, G.W., 1993. A finite-difference, time-domain solution for three-dimensional electromagnetic modeling, *Geophysics.* **58**, 797-809.

Wang, T. and Tripp, A.C., 1996. FDTD simulation of EM wave propagation in 3-D media, *Geophysics.* **61**, 110-120.

Weiss, C.J., 2007. The fallacy of the shallow-water problem in marine CSEM exploration, *Geophysics*. **72**, A93-A97.

Wang, M., Deng, M., Wu, Z., Luo, X., Jing, J. and Chen, K., 2017. The deep-tow marine controlled-source electromagnetic transmitter system for gas hydrate exploration, *Journal of Applied Geophysics*. **137**, 138-144.

Yee, K.S., 1966. Numerical solution of initial value problems involving Maxwell's equations in isotropic media, *IEEE Transactions on Antennas and Propagation*. **14**, 302-307.

Yin, C., Qi, Y. and Liu, Y., 2016. 3D time-domain airborne EM modeling for an arbitrarily anisotropic earth, *Journal of Applied Geophysics*. **131**, 163-178.

Yang, D., Oldenburg, D.W. and Haber, E., 2014. 3-D inversion of airborne electromagnetic data parallelized and accelerated by local mesh and adaptive soundings, *Geophys. J. Int.*. **196**, 1492-1507.

Zhdanov, M.S., 2009. *Geophysical Electromagnetic Theory and Methods*, Elsevier.

Zaslavsky, M., Druskin, V. and Knizhnerman, L., 2011. Solution of 3D time-domain electromagnetic problems using optimal subspace projection, *Geophysics*. **76**, F339-F351.

Appendix A. Analytical Solution of Horizontal Electric Dipole with Impulse Source

Given an horizontal electric dipole on the earth's surface (z=0) and a homogeneous halfspace, the frequency domain response of electric field (take E_x for example) on the earth's surface can be written as follows(Ward and Hohmann, 1988):

$$E_x = \frac{Ids}{2\pi}\frac{\partial}{\partial x}\left[\frac{x}{\rho}\int_0^\infty \frac{\lambda}{\hat{y}_1} J_1(\lambda\rho)d\lambda\right] - \frac{\hat{z}_0 Ids}{2\pi}\int_0^\infty \frac{\lambda}{\lambda + u_1} J_0(\lambda\rho)d\lambda \tag{A.1}$$

where I is the current of the electric dipole, ds is the length of the dipole, $\rho = \sqrt{x^2+y^2}$, $\lambda^2 = k_x^2 + k_y^2$, $u_1 = \sqrt{k_x^2 + k_y^2 - k_1^2}$, $k_1 = \sqrt{\mu\epsilon\omega^2 - i\omega\mu\sigma}$ is the wavenumber for homogeneous halfspace earth, $\hat{y} = \sigma + i\omega\epsilon$ is the admittivity, $\hat{z} = i\omega\mu$ is the impedivity, ω is the angular frequency, J_0 and J_1 are the Bessel function of the zero and first order.

By substituting $s = i\omega$ in the frequency domain expression, dividing by s, and take the inverse Laplace transform ($\mathcal{L}^{-1}$), one can find the time domain response caused by a step source. The analytical solution of the step response caused by a horizontal electric dipole has been given in Ward and Hohmann (1988). Similarly, the direct transformation of the frequency domain response generates the impulse response in time domain. The derivation of the analytical solution for impulse response is presented for vertical magnetic dipole source in Ward and Hohmann (1988). Here, we briefly discuss the derivation of impulse response for electric dipole source. We take the inverse Laplace transform of (A.1) to obtain the time domain response for impulse source:

$$E_x(t) = \frac{Ids}{2\pi}\frac{\partial}{\partial x}\left[\frac{x}{\rho}\int_0^\infty \mathcal{L}^{-1}(\frac{\lambda}{\hat{y}_1}) J_1(\lambda\rho)d\lambda\right] - \mathcal{L}^{-1}\left[\frac{\hat{z}_0 Ids}{2\pi}\int_0^\infty \frac{\lambda}{\lambda + u_1} J_0(\lambda\rho)d\lambda\right] \tag{A.2}$$

We now consider the first term in the right hand side of (A.2). By considering the following identity (Tu, 2015):

$$\mathcal{L}^{-1}(\frac{\lambda}{\hat{y}_1}) = \mathcal{L}^{-1}(\frac{\lambda}{\sigma + s\epsilon}) = \frac{\lambda}{\epsilon} e^{\frac{-\sigma t}{\epsilon}}, \tag{A.3}$$

we can obtain:

$$\int_0^\infty \mathcal{L}^{-1}(\frac{\lambda}{\hat{y}_1})J_1(\lambda\rho)d\lambda = \frac{1}{\epsilon}e^{\frac{-\sigma t}{\epsilon}}\int_0^\infty \lambda J_1(\lambda\rho)d\lambda = \frac{1}{\epsilon}e^{\frac{-\sigma t}{\epsilon}}\frac{1}{\rho^2} \tag{A.4}$$

where we also used the identity that $\int_0^\infty \lambda J_1(\lambda\rho)d\lambda = 1/\rho^2$

Follow this, we consider the second term in the right hand side of (A.2). After some simple substitution, we find that (Tu, 2015):

$$\frac{\hat{z}_0 Ids}{2\pi}\int_0^\infty \frac{\lambda}{\lambda+u_1}J_0(\lambda\rho)d\lambda = -\frac{Ids}{2\pi\sigma}\left[\int_0^\infty \lambda^2 J_0(\lambda\rho)d\lambda - \int_0^\infty \lambda u_1 J_0(\lambda\rho)d\lambda\right] \tag{A.5}$$

By considering the well-known Lipschitz's Integral and Somerfield identity (Ward and Hohmann, 1988), we can obtain the following equations:

$$\int_0^\infty \lambda^2 J_0(\lambda\rho)d\lambda = \frac{\partial^2}{\partial z^2}\left(\frac{1}{r}\right) \tag{A.6}$$

$$\int_0^\infty \lambda u_1 J_0(\lambda\rho)d\lambda = \frac{\partial^2}{\partial z^2}\left(\frac{e^{-ik_1 r}}{r}\right) \tag{A.7}$$

where $r = \sqrt{\rho^2+z^2} = \rho$ (considering that z=0).

By substituting equations (A.4),(A.5), (A.6),(A.7) into equation (A.2); after some simplification, we can obtain the time domain response for the impulse source as follows (Tu, 2015):

$$E_x(t) = \frac{Ids}{2\pi\epsilon}e^{-\sigma t/\epsilon}\left(\frac{3x^2}{\rho^5}-\frac{1}{\rho^3}\right) + \frac{Ids}{8}\left(\frac{\mu^3\sigma}{\pi^3 t^5}\right)^{\frac{1}{2}} e^{-\frac{\mu\sigma\rho^2}{4t}} + \frac{Ids}{2\pi\sigma\rho^3}\delta(t). \tag{A.8}$$

In the derivation, we have used some other basic properties of Laplace transforms, for example:

$$\mathcal{L}^{-1}\left(e^{-k\sqrt{s}}\right) = \frac{k}{2\sqrt{\pi t^3}}e^{-\frac{k^2}{4t}}, k>0 \tag{A.9}$$

Due to the page limits, we will not list all these properties in this derivation.

Highlights

- This paper develops a finite element time domain algorithm for 3D CSEM modeling
- We proposed a hybrid condition to reduce the size of problem
- The finite element system of equations is solved using direct solver
- The developed method is effective in modeling complex geometry such as bathymetry